ADVANTAGES OF IN SITU DATA WHEN ESTIMATING THE GLOBAL NEUTRAL ATMOSPHERIC DENSITY USING A DATA ASSIMILATION SYSTEM

C. F. Minter[(1)], T. J. Fuller-Rowell[(1)], M. V. Codrescu[(1)]

[(1)]Cooperative Institute for Research in Environmental Sciences, University of Colorado, NOAA/SEC, 325 Broadway, Boulder, CO 80305, USA, Cliff.Minter@NOAA.gov, Tim.Fuller-Rowell@NOAA.gov, Mihail.Codrescu@NOAA.gov.

ABSTRACT/RESUME

Recently developed data assimilation techniques have improved time-dependent estimates of the neutral atmospheric density, making it possible to better estimate the drag perturbation force on low-Earth-orbiting satellites. These new systems primarily use surveillance of a satellite's orbital parameters to determine the neutral density along the satellite's flight path. A limitation to satellite surveillance comes from the need to observe each satellite over long periods (hours) to determine the satellite's average acceleration change. This limitation in temporal and spatial resolution translates into limited resolution in the data assimilation solution. In situ data, on the other hand, provide density measurements with a substantially increased temporal and spatial resolution. Evaluations show that, even though the global coverage from in situ sources is typically limited (usually 2 or fewer satellites) as compared with a constellation (50+) for satellite surveillance, the higher temporal and spatial resolution of in situ data minimizes errors and increases the resolution of the data assimilation output. Furthermore, the higher temporal and spatial resolutions of in situ data are shown to be especially important during geomagnetic storms when changes in the neutral density can occur on a minute-to-minute basis. Results of the data assimilation system are used to compare the use of satellite surveillance and in situ data with emphasis on CHAMP data.

1. INTRODUCTION

After the oblateness of the Earth, atmospheric drag is the second most significant natural perturbation force affecting satellite trajectories for low-Earth-orbiting (LEO) (<1000 km) satellites [1]. Further more, since the neutral atmosphere (95 to 500 km altitude) is constantly changing, estimating the drag perturbation has the largest uncertainty. The total neutral density affects a satellite's trajectory through the drag force described as

$$\boldsymbol{a}_{drag} = -\tfrac{1}{2} C_D A \rho \boldsymbol{v}_{rel} |\boldsymbol{v}_{rel}| / m \qquad (1)$$

where $\boldsymbol{a}_{drag}$ is the perturbing acceleration, C_D is the dimensionless value for the drag coefficient and dependent on the shape of the satellite, A is the satellite's cross-sectional area, and m is the mass of the satellite. The vector, $\boldsymbol{v}_{rel}$, represents the satellite's velocity relative to the atmosphere, and ρ is the total mass density of the atmosphere. Although difficulties arise in estimating all of the terms in the drag force equation (1), the density term, ρ, is often among the largest sources of uncertainty. Any improvement in estimating of ρ would significantly improve the drag estimate and consequently improve one's estimate of the other orbital parameters, as tests have shown [2,3]. One should note that equation (1) is a simplification of a much more complicated process of translating the atmospheric density into the amount of force experienced by the spacecraft. At the altitudes discussed in this paper, equation (1) is complicated when applied to rarified and ionized gases. Spacecraft shape and constantly changing orientation further complicate the translation from density to drag. The research presented here will only discuss estimating the density, ρ. Translating ρ to perturbing acceleration is beyond the scope of this paper.

Empirical, or static models, of the upper atmosphere, like the Jacchia 70 [4], Jacchia 77 [5], the Mass Spectrometer and Incoherent Scatter Extension (MSIS-E-90) [6, 7, 8] and the Naval Research Laboratory MSIS (NRLMSIS-00) [9] models, are a convenient way to represent ρ. These models provide a quickly calculable empirical solution according to a combination of defined and observed parameters, based on a statistical representation of the neutral atmospheric density obtained from years of satellite, rocket, and ground observations. Unfortunately, because the empirical model is statistical representation of the climate over a long period of time (years, months), they may not appropriately represent unusual, short-term features (hours, minutes) in the upper atmosphere. The complex process of heating in the upper atmosphere, which is further complicated during geomagnetic storms, often produces unusual features that may not be aptly described empirically. Recent studies [10] indicate that the required density correction for NRLMSIS-00 has reached 30% at 200 km altitude and 70% at 600 km altitude, for example.

The simulation presented in this research uses MSIS-E-90 to provide the nominal state vector in the batch least squares process. Both empirical models, MSIS-E-90 and Jacchia 70, provide temperature, from which the density at a given altitude can be obtained [11]. For the scope of this study, either model could have been chosen. Although Jacchia 70 is used in the High Accuracy Satellite Drag Model (HASDM) [11], MSIS-

E-90 is chosen to represent the nominal state due to its ease of use in the least squares solution software.

One should keep in mind that, although empirical models may be imperfect, these models still provide the best representation of the neutral density without recent observations. With recent observations, however, the current best representation can be further improved my implementing a least squares solution, which calculates a solution for the state based on the minimization of the sum of squares of the observation errors [12, 13, 14], to make the statistically optimal correction. The results will show that the neutral atmospheric density can be specified to a high accuracy by making corrections to an empirical model using either ballistic coefficient estimation or in situ measurements through the batch least squares solution. The two observing platforms, ballistic coefficient estimation and in situ measurements, will be compared by quantifying how well each can reproduce a defined 'truth' neutral atmosphere according to each observing platform's mechanics and satellite definitions. The quality of the least squares solution in reproducing the 'truth' file will be scored on its root mean square error, to provide a globally averaged error as an indication of how well the solution matches the true neutral density structure.

2. OBTAINING THE DENSITY THROUGH BALLISTIC COEFFICIENT ESTIMATION

Based on the concept of making corrections to an empirical model using observations, a data assimilation system, called the High Accuracy Satellite Drag Model (HASDM) [3, 11, 15, 16, 17, 18, 19] is currently in use. HASDM has demonstrated the ability to significantly reduce the error in total density in the empirical model during quiet geomagnetic conditions.

As in all data assimilation systems, the state must be observed to be corrected. The HASDM system infers the density specification by space surveillance of the orbits of a given constellation of satellites. By estimating the acceleration parameter of each satellite, an estimated ballistic coefficient, B_{est}, can be obtained from the drag force equation (1). The ballistic coefficient portion of the drag force equation is written as

$$B_{est} = C_D A/m\,, \tag{2}$$

which is estimated for each satellite. The estimated ballistic coefficient is compared to each satellite's 'known' ballistic coefficient, B_{known}, which is known within a small error [17, 18]. From this comparison, a correction to the empirical model total density is made by adjusting the model solution, $\rho^*(t)$, according to the ratio between the estimated, B_{est}, and known, B_{known}, ballistic coefficients. The corrected state, $\rho(t)$, representation of neutral density at a given time, t, can be described as

$$\rho(t) = \rho^*(t) B_{est} / B_{known}\,. \tag{3}$$

As the neutral atmospheric density changes with time, these changes are reflected in the satellite's acceleration term. New observations of this term provide updated estimates of the estimated ballistic coefficient and subsequent corrections to the neutral atmospheric density solution, allowing for a time-dependent representation of the density.

HASDM uses an empirical model to provide a nominal state and subsequently estimates the deviation from the nominal state, based on the densities obtained from the drag force equation (1) and the ballistic coefficient estimates. The estimated deviation is added to the nominal state to provide the statistically best estimate of the neutral density through a batch least squares solution. HASDM's use of a large satellite constellation as an observation platform improves the total coverage, ensuring that observations from many regions of the globe are included in the solution process. Results, as will be shown later, demonstrate that the higher global coverage provides greater accuracy for the first order estimate of the neutral atmospheric density. Results, in this paper and in another study [19], show that, when using ballistic coefficient estimation from a large (60) satellite constellation as the observing scenario, the batch least squares will provide a well-conditioned solution with a spherical harmonic resolution of degree and order 2 to 3.

Although ballistic coefficient estimates from 60 satellites provide a large global coverage of the neutral atmosphere, resolving the density structure from these estimates is difficult. The difficulty comes from observing the satellite's trajectory over long periods, 3 segments of 6 hours each, 18 hours total, to reduce noise in the observation data set. To discriminate the ballistic coefficient from the noise, a spline is computed over the 18-hour observation interval, which is divided into three 6-hour parts [11, 16]. In HASDM, the middle 6 hours has 2/3 of the weighting, and the 6-hour segments on either end of the interval have 1/6 of the weight. The time-dependent neutral atmospheric structure within each 6-hour period is obtained from the corrected time-dependent empirical model.

In order to compare with other techniques, the HASDM-type system is reproduced here. This study assumes that the HASDM-type system obtains the ballistic coefficients from the 60 satellites. This system is the control case for comparison against the in situ observing technique. The parameters for the 60 satellites used for ballistic coefficient estimation, are identical to those used in HASDM [19].

Various levels of noise in observing the ballistic coefficients were examined in this research, but the noise level showed little effect on the solution accuracy since the spline removes much of the observation noise before the observations are ingested by the least squares solution. The spline fit is basically an averaging technique, and different noise levels still have the same

mean as long as no bias exists. It is this mean that is used as the ingested observations used by the least squares method. In this research, however, it is assumed that a 1% observation error exists in the ballistic coefficient estimate. Various error levels, up to 20%, were tested, but each solution provided almost identical results. The low error of 1% is chosen since it represents a 'best case' representation of a data assimilation system using ballistic coefficient estimates, although the error has little effect on the solution accuracy.

3. SOLUTION METHOD

A data assimilation system, similar to the mechanics of HASDM, is constructed based on the technique of batch least squares. In HASDM, the state vector, containing the spherical harmonic coefficients, can describe either the total neutral density or the temperature at a given location and altitude, since density, temperature, and altitude are functionally related. The current version of HASDM observes the neutral density through ballistic coefficient estimates. However, the data assimilation system applied in this research may acquire observations of the density through either ballistic coefficient estimates via space surveillance or in situ measurements. When using ballistic coefficient estimates as the observation set, the system operates similarly to HASDM and acts as the control case. The batch least squares equations, described in this section, are equivalent for both observing platforms with the exception of the observation equations.

Least squares, in summary, calculates a solution for the state based on the minimization of the sum of squares of the observation errors. The batch least squares solution [12, 13, 14] is generalized for the problem presented here as

$$\hat{\boldsymbol{X}}_k = \left(H_k^T R_k^{-1} H_k + \overline{P}_k^{-1}\right)^{-1}\left(H_k^T R_k^{-1}\left[\boldsymbol{y}_k - \boldsymbol{y}_k^*\right] + \overline{P}_k^{-1}\left[\overline{\boldsymbol{X}}_k - \boldsymbol{X}_k^*\right]\right) + \boldsymbol{X}_k^* \cdot \quad (4)$$

where y_k represents the observation data, and $\boldsymbol{y}_k^*$ contains the expected observations based on the defined nominal state. The state vectors include the following: $\overline{\boldsymbol{X}}_k$, the *a priori*, or best estimate of the state before the least squares calculation is performed; $\boldsymbol{X}_k^*$, the nominal state; and $\hat{\boldsymbol{X}}_k$, the new least squares estimate for the state for a given batch of observations at a given epoch, *k*. The *a priori* state, $\overline{\boldsymbol{X}}_k$, can contain either the initial conditions, which are usually obtained from the defined nominal state, or the current state estimate based on a previous batch of data. Associated with the *a priori* state is the *a priori* error variance-covariance matrix, $\overline{P}_k$, whose diagonals are an indicator of the amount of error variance in the state. The off-diagonal terms in $\overline{P}_k$ indicate the amount of covariance between any two elements in $\overline{\boldsymbol{X}}_k$. $\overline{P}_k$ is initialized based on the expected amount of error in the nominal state. The error variance-covariance matrix can be updated with each new batch of data as

$$P_k = \left(H_k^T R_k^{-1} H_k + \overline{P}_k^{-1}\right)^{-1} \quad (5)$$

where P_k is the new state error variance-covariance matrix based on the new state from least squares result. After the new state, $\hat{\boldsymbol{X}}_k$, and its associated error variance-covariance matrix, P_k, are calculated, this state and associated error matrix replace the *a priori* state, $\overline{\boldsymbol{X}}_k$, and the *a priori* state error variance-covariance matrix, $\overline{P}_k$, in equations (4) and (5). The least squares solution may be recalculated to provide an improved solution. The solution can be further improved by iterating this process. No substantial improvement is seen in the least squares solution after about 2 to 3 iterations.

As defined earlier, the observation vector, y_k, contains all observations in a given batch, whether ballistic coefficient estimates or in situ measurements. Associated with the observation vector, R_k is the observation error variance-covariance matrix that contains an estimate of the variance uncertainty in y_k. R_k is estimated before the least squares method is applied. The diagonals of R_k represent the error variance in the observations defined by the instrument and observation system accuracy. The off-diagonals in R_k are assumed to be 0. The expected observation vector, $\boldsymbol{y}_k^*$, contains the observations that one would expect given the nominal state at the epoch, *k*.

If the state vector and the observation can be related in a linear manner, the state may be translated, or mapped, back to the observation vector through the matrix, H_k, which is often referred to as the 'mapping matrix'. H_k contains the linearized observation equations and describes the relationship between the observation and the state estimate as

$$\boldsymbol{y}_k = H_k \hat{\boldsymbol{X}}_k + \boldsymbol{\varepsilon}_k$$

where ε_k is the error on the observation. Although $\hat{\boldsymbol{X}}_k$ is the same for both observing platforms, y_k is observation platform dependent since it contains either the ballistic coefficient estimates or density inferred from the ultra-violet airglow emissions. H_k must be accordingly representative of the relationship between $\hat{\boldsymbol{X}}_k$ and the different observation vectors for y_k. Other than H_k, y_k, and R_k, the batch least squares vectors, matrices, and equations are the same for both observing platforms.

The elements in $\hat{\boldsymbol{X}}_k$ represent the coefficients of a series of spherical harmonics representing the neutral atmospheric temperature or total density. The value for the neutral density, ρ, for example, at a specific latitude,

ψ, and longitude, λ, expanded in spherical harmonics [20], may be written as

$$\rho(\psi,\lambda) = a_0 + \sum_{i=1}^{\infty} a_i [P_i(\sin\psi)] + \sum_{i=1}^{m}\sum_{j=1}^{i} [P_{i,j}(\sin\psi)]\{c_{i,j}\cos(j\lambda) + s_{i,j}\sin(j\lambda)\} \quad (6)$$

The spherical harmonic equations and the estimates of the associated coefficients allow for a functional representation of the density at any point on the globe. Although the structure of the neutral atmospheric density is varied, the neutral density structure is also naturally continuous, and therefore, implementing the continuous function using the spherical harmonics is an ideal representation.

4. EVALUATING THE TWO OBSERVING PLATFORMS

To evaluate the two density observing techniques, a simulated 'truth' neutral atmosphere is defined using the Coupled Thermospheric-Ionospheric Model, CTIM [21, 22, 23, 24]. This 'truth' neutral atmosphere is sampled according to the satellite and instrument mechanics for the observing platform under consideration, 60 satellites for ballistic coefficient estimation or 2 in situ satellites, using a satellite/instrument simulation algorithm [25].

The physical model used to create the 'truth' neutral atmosphere, CTIM, is a combination of two independently developed physical models driven by a Foster-type electric field [26]. The first part of CTIM contains a global, non-linear, time-dependent neutral atmospheric model developed at University College London [21, 22, 23, 24]. The second part contains a mid- and high-latitude ionospheric convection model that originated at Sheffield University [24]. The high latitude electric field and auroral particle precipitation are the two main high latitude inputs for the ionospheric-thermospheric coupled model, and these inputs determine the amount of Joule heating. The other main input is the solar ultraviolet and extreme ultraviolet radiation which provide the bulk of the thermospheric heating and ionozation.

CTIM was chosen to simulate the 'truth' neutral atmosphere since the code solves the non-linear equations of momentum, energy, and continuity to provide a time-dependent structure of the wind vector, temperature, and density in the neutral atmosphere. As a result, the simulation from a physical model would provide a more varied, detailed, and realistic structure in comparison to the statistically averaged structure provided by empirical models. This difference in structure between the empirical and physical model types would resemble the expected differences between the empirical models and reality. From this type of comparison, a more stringent and realistic test is created for the two observation platforms and the data assimilation system.

For results comparison, the batch least squares solution for both observing platforms is scored on how well it reproduces the CTIM 'truth' set through a standard root mean square error. The RMS error between the truth file and the least squares estimated state is calculated as

$$\text{RMS} = \sqrt{\sum_{i=1}^{n} [(\hat{\rho}_i - \rho_i^{CTIM}) A_i / \overline{A}]^2 / n} \quad (7)$$

where $\hat{\rho}_i$ is the estimated density at a particular grid point, *i*, and ρ_i^{CTIM} is the corresponding i^{th} grid point of the CTIM-defined truth density. A_i is the area associated with grid point *i*, based on a 91x20 lat-long grid - 2 degrees latitudinal and 18 degrees longitudinal spacing. $\overline{A}$ is the average area of all of the grid points and is included to normalize the RMS error result, and *n* is the total number of grid points.

5. ILLUSTRATIVE EXAMPLE

A 2-day period, March 21-22, is simulated to provide the test case. An equinox scenario provides a thermosphere where roughly equal heating of the Southern and Northern Hemispheres exists. The test case simulates a 24-hour period of low geomagnetic activity with an energy input of about 10 GW, which is approximately equal to an *Ap* index of about 7. After the 24-hour quiet period, a 12-hour geomagnetic storm with a power input of about 260 GW follows, equivalent to an *Ap* index of approximately 300. After this 12-hour storm period, another 12-hour quiet time period, with an *Ap* of 7, follows. The total simulation period covers 48 hours. The results, during the quiet period from 0 to 24 hours, demonstrate the quiet-time accuracy of the least squares solution under undisturbed conditions. At 24 hours, the geomagnetic storm commences. During the 12-hour storm period, from hour 24 to 36, the data assimilation system must then react to a rapidly changing state. The final 12 hours of quiet, from hour 36 to 48, demonstrate the recovery characteristics of the least squares solution, during which the composition is still changing as it recovers from the storm to quiet conditions.

The first test of the data assimilation system provides a control case and resembles HASDM in that the data assimilation system estimates the neutral density from ballistic coefficient estimates. This first portion of the simulation uses the 60 LEO satellites, which have the same orbital parameters as in HASDM.

The second observation platform type uses in situ measurements. The in situ platform considers various combinations of two satellites at separate local time crossings. Both in situ satellites are simulated to take one measurement every 10 seconds. The measurement error of the temperature is assumed to have a standard deviation roughly 1% for both in situ satellites.

In all of the examples, MSIS-E-90 is defined as the nominal state, unless specified otherwise. Differences from this nominal state are estimated using the batch least squares method. These differences are then added

to the nominal state to obtain the neutral density specification.

To quantify the average global accuracy of the data assimilation system, the RMS over the entire globe is computed, according to equation (7), for both observing platforms. The results, using the ballistic coefficient estimates, are shown in Fig. 3.

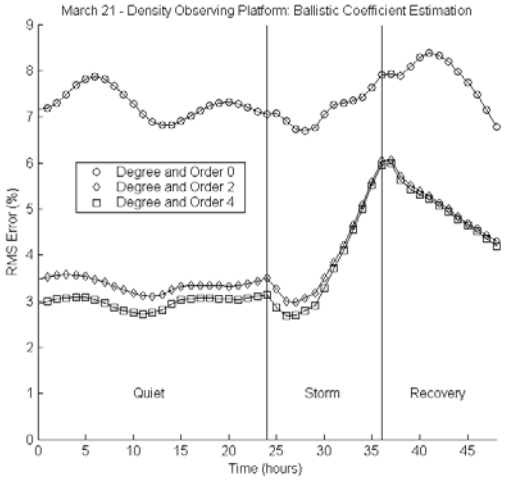

FIG 3. Time-dependent RMS errors for ballistic coefficient estimation using 60 satellites for varying spherical harmonic resolutions.

Varying spherical harmonic resolutions are shown for the least squares solution for the ballistic coefficient estimation platform in Fig. 3. The ballistic coefficient estimation results, in Fig. 3, show similar error levels in comparison to HASDM [15], and the accuracy does not significantly improve when the degree and order of the spherical harmonic resolution is increased beyond degree/order 2. The best results for the ballistic coefficient platform show an RMS error consistently below 4% during geomagnetic quiet times but also show about a 3% increase in the RMS error, to 6%, by the end of the 12-hour storm. This sudden increase in the RMS error during the geomagnetic storm may be the result of the poorer temporal resolution of the ballistic coefficient platform. Although the global coverage is high, sudden storm-induced changes in the neutral atmosphere occur more rapidly than can be estimated by the least squares solution when ballistic coefficient estimation is used.

The RMS errors for the in situ observing platform are shown in Fig. 4. The figure shows that the RMS errors also decrease as the spherical harmonic degree and order increase beyond 2, indicating that the higher temporal resolution of in situ measurements allows for a better conditioned solution for the least squares inversion. In situ measurements demonstrate low RMS errors despite having a coverage of only two satellites. For degree/order 4, the in situ platform results show errors consistently below 3% during geomagnetic quiet times. Perhaps more importantly, the geomagnetic storm errors do not rise as sharply as in Fig. 4, when compared to the ballistic coefficient storm results in Fig. 3. RMS Errors, for the in situ platform for degree/order 4 in Fig. 4, remain below 4% throughout the 12-hour storm. The lower RMS error, during the storm period for the in situ measurements, shows that, although the global coverage for 2 satellites is poorer, the higher temporal resolution outweighs the loss in coverage by capturing the storm-induced sudden changes in a timely manner.

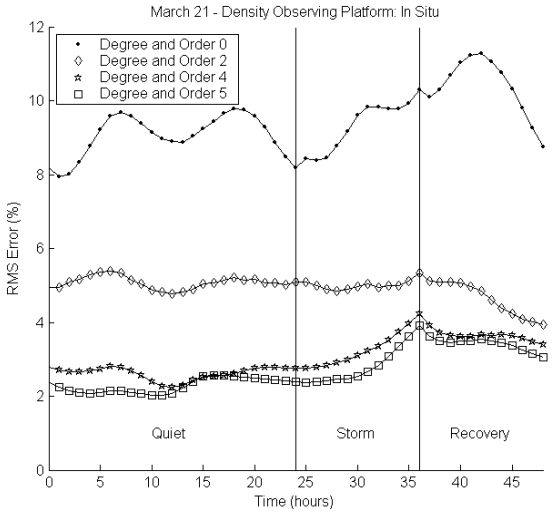

FIG 4. Time-dependent RMS errors for the in situ simulation using a two sun-synchronous satellites at 09:30 and 13:30 LT crossing for varying spherical harmonic resolutions.

Figure 3 verifies the results found in the HASDM analyses, demonstrating that using ballistic coefficient estimation does not significantly improve after degree/order 2. The same result is not necessarily true for the in situ platform according to Fig. 4 as improvements in the resolution continues to increase beyond degree and order 2. This result may be explained by the conditioning of the least squares solution. If the observation sampling is sparse in comparison to the number of parameters to be solved, a linear dependence occurs in the system of equations whose solution is required in the determination of the spherical harmonic coefficients [27, 28]. Under these conditions, the problem is considered ill-conditioned, and the solution may be inaccurate for increasingly higher order terms in the spherical harmonic representation. Although the 60 HASDM satellites have a uniform distribution over the globe, obtaining the ballistic coefficient estimate from an 18-hour track of these satellites can make the system ill-conditioned as the number of spherical harmonic coefficients to be solved increases. The inclusion of higher order coefficients beyond degree/order 2, makes the matrix, $H^T R^{-1} H + \overline{P}_k^{-1}$, to be inverted in equation (4), increasingly more linearly dependent, and numerical

errors are introduced as the degree and order increase. The state error variance-covariance matrix, $\overline{P}_k$, helps stabilize the inversion, but for ill-conditioned systems, the solution is very sensitive to the choice for $\overline{P}_k$ [29]. Providing an accurate estimate for $\overline{P}_k$ may be difficult, particularly if $\overline{P}_k$ is constantly changing with the dynamic neutral atmosphere. On the other hand, despite the poorer global coverage from only 2 in situ satellites, the least squares equation is still well-conditioned when higher order terms are included due to the higher temporal resolution. In effect, the higher temporal resolution leads to a higher spatial resolution in the least squares solution representing the neutral atmospheric density structure.

For the first order correction to the empirical model of degree/order, observing the neutral density using ballistic coefficient estimation provides a lower RMS error of about 7-8.5%, as shown in Fig. 3 - as opposed to 8-9% in Fig. 4 when in situ measurements used. When using ballistic coefficient estimation, the first order correction to the empirical model, degree/order 0, the results are more accurate since the global coverage is more uniform when 60 satellites are used. Consequently, a more accurate global mean is calculated as compared to the two satellites in in situ. The first order correction using ballistic coefficient estimation is shown in the middle panel in Fig. 5 in the form of exospheric temperature. Hour 18 is chosen to illustrate the differences between the degree/order 0 RMS errors, in Fig. 3 and Fig. 4, for the ballistic coefficient estimation and in situ platforms, respectively. The 'truth' neutral temperature is shown in the top panel. The bottom panel provides the absolute error between 'truth', top panel, and the least squares result in the middle panel. The absolute error, in the bottom panel, indicates a maximum temperature deviation of about 220 K at about 290 degrees to 10 degrees longitude and between $\pm$ 45 degrees latitude. In most other regions, however, the error in the bottom panel is low, between 0 and 50 K.

Even though, for in situ, the global distribution of observations is poor, the simulation results using in situ measurements show comparable, and sometimes slightly better, results compared to ballistic coefficient estimation when higher order terms are used in the spherical harmonic representation. The temporal resolution of in situ measurements, as already mentioned, is significantly higher, and the spatial resolution of the region under observation is therefore significantly increased, making the inverse in equation (4) well conditioned beyond degree/order 2 despite the limited global coverage. The differences between the two observing platforms are illustrated in Fig. 5 and Fig. 6 where best ballistic coefficient resolution and the best in situ resolution, degree/order 4, are shown respectively, at the geomagnetic storm's end at hour 36.

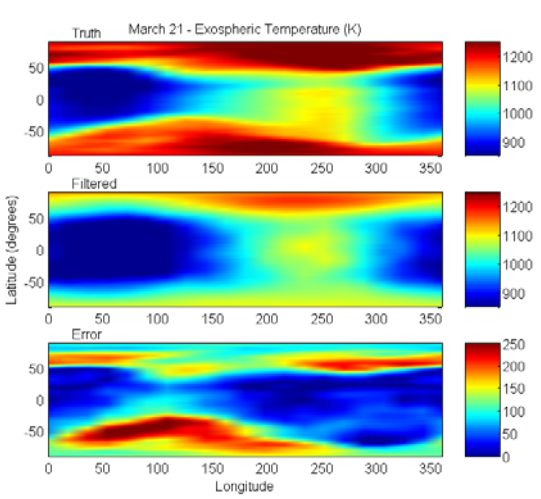

FIG 5. Exospheric temperature by ballistic coefficient estimation using 60 satellites for degree/order 4 spherical harmonic resolution at hour 36.

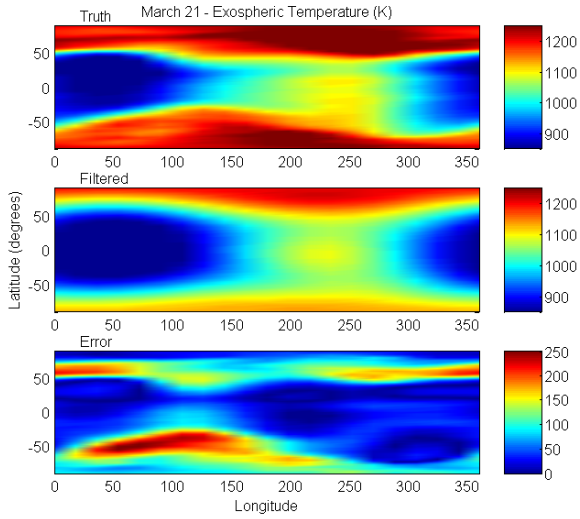

FIG 6. Exospheric temperature by in situ using two sun-synchronous satellites at 09:30 and 13:30 LT crossing for degree/order 4 spherical harmonic resolution at equinox at hour 36.

The middle panels of Fig. 5 and Fig. 6 respectively show the ballistic coefficient estimation and in situ least squares results with their respective absolute errors in the bottom panels of both figures. The 'truth' neutral atmosphere representations, in the top panels of Fig. 5 and Fig. 6, are by definition identical. The differences, however, between the ballistic coefficient estimate and in situ platforms are shown in their least squares solution results, in the middle panels, and their absolute errors, bottom panels. The middle panel of Fig. 5, illustrating the solution using ballistic coefficients, also shows an underestimate of the high latitude temperature. The true temperature, shown in the top panels, above

±50 degrees latitude, ranges between 1,200 and 1,300 K. The least squares solution, for the ballistic coefficient estimation platform in the middle panel of Fig. 5, ranges between 1,100 and 1,200 K above ±50 degrees latitude. This error is reflected in the bottom panel of Fig. 5 where the absolute error at the higher latitudes is often above 200 K as indicated by the large red areas. The ballistic coefficient estimation result may have larger errors at the higher latitudes since the coverage is not uniformly distributed. Although, most of the HASDM satellites are beyond ±50 degrees inclination, 11 of the 60 satellites are within ±50 degrees inclination. Satellites with a high inclination angle can cover most latitudes, but smaller inclination angles limit satellite coverage to only the middle latitudes. Therefore, the accuracy may be slightly higher in the middle to low latitudes for the ballistic coefficient estimation results.

The middle panel of Fig. 6 shows the least squares result when using two sun-synchronous in situ satellites at 09:30 and 13:30 LT crossings. The in situ results seem to capture the neutral atmospheric structure with slightly better accuracy in the higher latitude regions. The middle panel shows a better representation, with temperature ranges between 1,150 and 1,250 K, of the true neutral atmospheric structure in top panel, with a temperature range of 1,200 and 1,300 K. The least squares result using in situ measurements is still underestimating the true temperature, but the absolute error is lower as reflected in the bottom panel of Fig. 6. The areas, having errors consistently above 200 K as shown in the bottom panel of Fig. 5 for the ballistic coefficient solution, are noticeably reduced in the bottom panel of Fig. 6 for the in situ case.

The least squares solutions for both observing platforms, in the middle panels of Fig. 5 and Fig. 6, show a very 'smooth' representation of the more varied 'truth' neutral atmosphere in the top panels. This smooth appearance comes from the inability to increase the least squares solution resolution by increasing the degree and order of the spherical harmonic representation because of the numerical errors discussed earlier. Obtaining a higher global resolution would require either an increase in the temporal resolution of the ballistic coefficient estimation technique or an increase in in situ coverage.

In summary, the in situ results provide more than a 1% improvement, at the storm's end, as compared to determining the neutral density using ballistic coefficient estimates from the 60-satellite constellation. This improvement for in situ over ballistic coefficient estimation indicates that the higher temporal resolution of in situ measurements are more influential in reducing these errors during geomagnetic storms. During geomagnetic quiet conditions, with the exception of storm recovery, both observation platforms perform similarly.

6. CONCLUSIONS

The research presented here demonstrates the effectiveness of estimating the total density using the two observing techniques: ballistic coefficient estimation and in situ. Both methods demonstrate the ability to significantly reduce errors in the total neutral density specification by correcting an empirical model. For the ballistic coefficient platform, errors remain consistently below 4% during quiet times and below 6% throughout a 12-hour simulated geomagnetic storm. When determining the total neutral density through ballistic coefficient estimation, the results verify the capability of the HASDM system, with a similar spherical harmonic resolution limit of degree and order 2. The limit in spatial resolution is an artifact of the reduced temporal resolution in the observation from having to observe the satellites over a long period to obtain their ballistic coefficients with sufficient precision. Although the global coverage is higher with 60 satellites, the ill-conditioning of the least squares solution is apparent when one attempts to increase the spherical harmonic representation beyond degree/order 2.

The use of 2-satellite in situ for obtaining the total neutral density showed improvement, over ballistic coefficient estimation, with errors consistently below 3% during geomagnetic quiet times and typically below 4% error during storm times. Overall, in situ showed a 1 to 2 % decrease in RMS error. However, although the global coverage is much less uniform for 2 in situ satellites as compared to 60 satellites for ballistic coefficient estimation, the higher temporal resolution for in situ allows a better least squares solution for the calculation of higher order spherical harmonic coefficients through the least squares solution without introducing numerical errors. Observing the density via in situ allows one to obtain an accurate specification, although variations in the RMS errors indicate that some features, particularly during geomagnetic storms, may remain unobserved.

7. REFERENCES

1. Vallado, D. A., *Fundamentals of Astrodynamics and Applications*, McGraw-Hill Companies, Inc., New York, Pages 485-525, 1997.
2. Marcos, F. A., Bass, J. N., Larson, D. R., Liu, J. J., and Robinson, E. C., "Satellite Drag Model Calibration and Feedback for Precision Low Earth Orbit Determination", Proceedings of the 1997 Space Control Conference, MIT Lincoln Laboratory, L. B. Spence, ed., Lexington, Massachusetts, 1997.
3. Marcos, F. A., Kendra, M. J., Griffin, J. M., Bass, J. N., Larson, D. R., and Liu, J. J., "Precision Low Earth Orbit Determination Using Atmospheric Density Calibration", *The Journal of the Astronautical Sciences*, Volume 46, Number 4, Pages 395-409, October-December 1998.

4. Jacchia, L. G., "Revised Static Models of the Thermosphere and Exosphere with Empirical Temperature Profiles", Smithsonian Astrophysical Observatory Special Report, Number 313, 1970.
5. Jacchia, L. G., "Thermospheric Temperature, Density, and Composition: New Models", Smithsonian Astrophysical Observatory Special Report, Number 375, 1977.
6. Hedin, A. E., 'Extension of the MSIS Thermosphere Model into the Middle and Lower Atmosphere', *Journal of Geophysical Research*, Volume 96, Number A2, Pages 1159-1172, February 1, 1991.
7. Hedin, A. E., "MSIS-86 Thermospheric Model", *Journal of Geophysical Research*, Volume 92, Number A5, Pages 4649-4662, May 1, 1987.
8. Hedin, A. E., "A Revised Thermospheric Model Based on Mass Spectrometer and Incoherent Scatter Data: MSIS-83", *Journal of Geophysical Research*, Volume 88, Pages 10,170-10,188, 1983.
9. Picone, J. M., Hedin, A. E., Drob, D. P., and Aikin, A. C., NRLMSISE-00 empirical model of the atmosphere: Statistical comparisons and scientific issues, J. Geophys. Res., 107(A12), 1468, 2002.
10. Yurasov, V. S., Nazarenko, A. I., Cefola, P. J., and Alfriend, K. T., "Density Corrections for the NRLMSIS-00 Atmosphere Model", AAS/AIAA Space Flight Mechanics Conference, AAS 05-168, Copper Mountain, Colorado, Page 9, January 23-27, 2005.
11. Storz, M., Bowman, B., and Branson, J., "High Accuracy Satellite Drag Model (HASDM)", AIAA/AAS Astrodynamics Specialist Conference and Exhibit, Monterey, California, August 5-8, 2002.
12. Lawson, C. L., and Hanson, R. J., *Solving Least Squares Problems*, Prentice Hall, 1963.
13. Liebelt, P. B., *An Introduction to Optimal Estimation*, Addison-Wesley, New York, 1967.
14. B. D. Tapley, B. E. Schutz, and G. H. Born, "Chapter 4: Fundamentals of Orbit Determination: The Sequential Estimation Algorithm", *Statistical Orbit Determination*, Academic Press, 2004.
15. Wise, J. O., Marcos, F. A., Bowman, B., Kendra, M. J., and Bass, J. N., "AFRL Neutral Density Support to HASDM", AIAA/AAS Astrodynamics Specialist Conference and Exhibit, Monterey, California, August 5-8, 2002.
16. Storz, M. F., "HASDM Validation Tool Using Energy Dissipation Rates", AIAA/AAS Astrodynamics Specialist Conference and Exhibit, Monterey, California, August 5-8, 2002.
17. Bowman, B. R., "True Satellite Ballistic Coefficient Determination for HASDM", AIAA/AAS Astrodynamics Specialist Conference and Exhibit, Monterey, California, August 5-8, 2002.
18. Bowman, B. R., "Time Series Analysis of HASDM Thermospheric Temperature and Density Corrections", AIAA/AAS Astrodynamics Specialist Conference and Exhibit, Monterey, California, August 5-8, 2002.
19. Casali, S. J. and Barker, W. N., "Dynamic Calibration Atmosphere (DCA) for the High Accuracy Satellite Drag Model (HASDM)", AIAA/AAS Astrodynamics Specialist Conference and Exhibit, Monterey, California, August 5-8, 2002.
20. Hobson, E. W., *The Theory of Spherical and Ellipsoidal Harmonics*, Chelsea Publishing, New York, 1931, reprinted in 1965.
21. Fuller-Rowell, T. J., Codrescu, M. V., Moffet, R. J., and Quegan, S., "Response of the Thermosphere and Ionosphere to Geomagnetic Storms", *Journal of Geophysical Research*, Volume 99, Number A3, Pages 3893-3914, March 1, 1994.
22. Fuller-Rowell, T. J., and Rees, D., "A Three-Dimensional, Time-Dependent, Global Model of the Thermosphere", *Journal of Atmospheric Science*, Volume 37, Pages 2545-2567, 1980.
23. Fuller-Rowell, T. J., Rees, D., Quegan, S., Moffett, R. J., Codrescu, M. V., and Millward, G. H., "A Coupled Thermosphere-Ionosphere Model (CTIM)", *Solar-Terrestrial Energy Program: Handbook of Ionospheric Models*, Scientific Committee on Solar Terrestrial Physics (SCOSTEP) , Pages 217-238, August, 1996.
24. Quegan, S., Bailey, G. J., Moffett, R. J., Heelis, R. A., Fuller-Rowell, T. J., Rees, D., and Spiro, J., "A theoretical study of the distribution of ionization in the high –latitude ionosphere and plasmasphere: first results on the mid-latitude trough and the light ion trough", *Atmosphere Terrestrial Physics*, Volume 44, Pages 619-640, 1982.
25. Minter, C. F., "Thermospheric Composition Forecasting Using Kalman Filtering Techniques", Ph.D. Dissertation, University of Colorado, August 2002.
26. Foster, J. C., Holt, J. M., Musgrove, R. G., Evans, D. S., "Ionospheric Convection Associated with Discrete Levels of Particle Precipitation", *Geophysical Research Letters*, Volume 13, Pages 656-659, 1986.
27. Goldstein, M., "The Poorly Conditioned Data on Multiple Regression Procedures", *British Journal of Mathematical Psychology*, Volume 31, Pages 102-105, 1978.
28. Silvey, S. D., "Multicollinearity and Imprecise Estimation", *Technometrics*, Volume 11, Pages 539-552, October, 1969.
29. Cicci, D. A. and Tapley, B. D., 'Optimal Solutions of Unobservable Orbit Determination Problems", *Celestial Mechanics*, Volume 44, Pages 339-369, 1988.